HIGH RESOLUTION IMAGES OF HERBIG–HARO OBJECTS

A.C. Raga[1] and M. Mateo[1,2,3]

Astronomy Department
University of Washington

RESUMEN

Hemos realizado un análisis de la estructura de condensaciones de los objetos Herbig-Haro (H-H) HH 1, HH 2, HH 47A y HH 7-11 en base a imágenes CCD de banda angosta. Estos objetos muestran estructuras cualitativamente muy distintas, desde la compleja estructura de condensaciones de HH 2 hasta la casi total falta de estructura de HH 47A. Para obtener toda la información posible sobre la estructura espacial de la emisión, hemos tratado de deconvolucionar los efectos atmosféricos e instrumentales de nuestras imágenes CCD. Aunque mejores resultados fueron obtenidos para las imágenes con señal más fuerte, en todos los casos fue posible mejorar la resolución espacial, mostrando detalles de la estructura espacial de la emisión.

ABSTRACT

We carry out an analysis of the condensation structure of the Herbig-Haro (H-H) objects HH 1, HH 2, HH 47A and HH 7-11 as observed in narrow-band CCD images. These objects show qualitatively very different structures, ranging from the very complex, high contrast condensation structure of HH 2 to the almost complete lack of structure of HH 47A. In order to obtain as much information about the spatial structure of the emission as possible, we have tried to deconvolve the seeing profile from the CCD images. Though better results are obtained for the images with higher signal-to-noise ratio, in all cases a relative improvement of the spatial resolution is possible, showing details of the spatial distribution of the emission.

Key words: DIRECT IMAGES – HERBIG-HARO OBJECTS

I. INTRODUCTION

Narrow band CCD images of stellar formation regions have proved to be very useful for obtaining information about the morphology of stellar jets and Herbig-Haro (H-H) objects (see e.g., Mundt 1985; Strom *et al.* 1986; Reipurth *et al.* 1986). The spatial structure observed in most stellar outflows is quite complex, and it has proven to be quite difficult to construct theoretical models to explain the observations.

It is now quite clear that H-H objects (discovered independently by Herbig 1951, 1952 and Haro 1952, 1953) are associated with high velocity outflows from young stars or protostellar objects. Unfortunately, at this time the theoretical models of H-H objects are still at a somewhat primitive stage. Most of the calculations which have been carried out are based on four different basic scenarios:

1. The "interstellar nozzle" model of Cantó (1980),

in which an initially isotropic stellar wind travelling into a stratified medium is collimated, forming an elongated cavity that ends at a "hot spot".

2. The "shocked cloudlet" model of Schwartz (1978), in which the H-H objects correspond to bow shocks formed by a stellar wind which impinges on high density condensations (which were originally present in the surrounding medium).

3. The "interstellar bullet" model of Norman and Silk (1979), in which clumps of matter are ejected at high velocities from the near environment of the source.

4. The "jet" model of Dyson (1984) and Mundt (1985), in which a continuous outflow (jet) is ejected from the environment of the source.

Predictions from models based on these scenarios have been used quite extensively for comparisons with observed emission line intensities (Hartmann and Raymond 1984; Hartigan, Raymond, and Hartmann 1987) and line profiles (Choe, Böhm, and Solf 1985; Solf, Böhm, and Raga 1986; Hartigan, Raymond, and Hartmann 1987). Also, a few comparisons with observed emission line intensity maps have been attempted (Raga 1986; Cantó, Sarmiento, and Rodríguez 1986; Falle, Innes, and Wilson 1987; Raga and Mateo 1987, 1988; Raga *et al.* 1987).

An important problem of comparisons between pre-

1. Visiting Astronomer, KPNO, operated by AURA under contract from NSF.
2. Visiting Astronomer, CTIO, operated by AURA under contract from NSF.
3. Now at Mount Wilson and Las Campanas Observatories, Pasadena.

13

dicted and observed intensity maps of H-H objects is that because of the small angular size of most H-H object (typically of the order of 10″) the effects of the seeing are very drastic. In the past we have degraded the theoretical intensity maps by convolving them with a simulated seeing profile, and then compared them with observational intensity maps. This technique has sometimes proved to be at least moderately successful (Raga et al. 1987), but in other cases the effect of the seeing is so drastic that it is impossible to tell whether or not there really is any agreement between the theoretical results and the observations (Raga and Mateo 1987).

In a recent study of the HH 34 jet (Raga and Mateo 1988) we have taken the opposite approach: we have attempted to deconvolve the effect of the seeing from the observed width of the jet. We have used a technique of assuming model parametric functions (i.e., one-dimensional Gaussian functions) for the profile of the jet (perpendicular to the jet axis), convolving these functions with the seeing profile, and then fitting the convolved functions to the observed jet profile to determine the function parameters. This technique was appropriate for our study because we were only interested in carrying out a one-dimensional deconvolution of a supposedly singly peaked function (i.e., the intensity profile perpendicular to the jet axis).

In the more general case of complex one-dimensional functions or of two-dimensional images, the technique of assuming parametric model functions is no longer practical. In this paper we present results obtained by deconvolving the effects of the seeing (in an approximate way) from narrow-band CCD images with a technique of Fourier deconvolution. We find that the enhanced spatial resolution images which are obtained with this process are useful for obtaining more meaningful comparisons between observational and theoretical intensity maps.

II. OBSERVATIONS AND REDUCTION TECHNIQUES

We present a study of narrow-band CCD images of a few Herbig-Haro objects. Our observations consist of an Hα frame of HH 1 and 2, a [S II] 6717 frame of HH 7-11 (both obtained in November 1986 with the KPNO 2.1-m telescope), and a [S II] 6717 + 6731 frame of HH 46/47 (obtained in April 1986 with the CTIO 0.9-m telescope). Details of the observations are summarized in Table 1. The HH 1/2 frame was obtained in excellent seeing conditions (a FWHM of 0.88″, see Table 1), but the HH 46/47 and HH 7-11 were obtained under moderate seeing conditions (FWHM of 1.12″ and 1.63″, respectively). Because we want to carry out a study of the morphology of these objects, we have attempted to increase the spatial resolution of the CCD frames by trying to deconvolve the seeing profile.

Image reconstruction techniques have been extensively used in the past in the context of radio, IR and X-ray astronomical observations (see e.g., the review of Narayan and Nityananda 1986). Attempts to deconvolve the seeing profile from optical photographic images have also been carried out (Hawkins 1979). The deconvolution of the seeing profile from CCD images is somewhat problematic because of the relative low oversampling of the seeing profile obtained with most CCD camera + telescope combinations. We have found that in spite of this it is still possible to partly eliminate the effects of the seeing. Even though the spatial resolution can be improved only in a partial way, it appears to be worth the effort to try to obtain somewhat higher resolution images.

The main problem lies in the fact that our frames have a scale of only 0.38″/pixel (except for the HH 47A frame, which has a scale of 0.36″/pixel, see Table 1), so that the FWHM of the seeing profile corresponds to 2-4 pixels in all cases. Also a result of the low sampling is the fact that regions with steep intensity gradients in the "unsmeared" image (i.e. not smeared by the seeing profile) are unresolved.

This lack of oversampling results in very bad aliasing problems when Fourier transforms are carried out. Experiments with test functions show that even in the case of no noise contamination, a very large increase in the power of the Fourier components with frequencies close to, but somewhat lower than the Nyquist frequency occurs (the Nyquist frequency is equal to $1/(2\Delta X)$, where ΔX is the separation between pixels). This effect, which is a result of the unresolved large gradient regions of the function, is analogous to the Gibbs phenomenon (which,

TABLE 1

LOG OF CCD OBSERVATIONS

Object	Date (UT)	Telescope	Primary Emission Line	Total Exposure Time (sec)	Central λ of Filter (A)	FWHM of filter (A)	Seeing (FWHM) (in arcsec)	Scale (in ″/pixel)
HH 1/2	1986 Nov 21	KPNO 2.1 m	Hα	3600	6564	27	0.88	0.38
HH 47 A	1986 Apr 3	CTIO 0.9 m	[S II] (6717 + 31)	3000	6728	34	1.12	0.36
HH 7-11	1986 Nov 22	KPNO 2.1 m	[S II] 6717	4000	6713	10	1.63	0.38

for example, is typically observed in finite stepsize treatments of functions with discontinuities). A somewhat drastic (but effective) way of dealing with this problem is to filter the Fourier spectrum, eliminating the high frequency components, and in this way getting rid of the oscillations described above.

We have carried out the following process. We first calculate the Fourier transforms G and S of the two-dimensional image g and seeing profile s. We then calculate the spectrum of the deconvolved image h as:

$$H = \left(\frac{G}{S}\right) \times F ,$$
(1)

where F is a filter function designed to cut off the high frequency part of the spectrum. It is hard to decide what function to use as a filter. Brault and White (1971) suggest using an "optimum filter", which is designed to eliminate a high frequency noise contribution. In our case (because the signal-to-noise ratio of our images is generally very good) the noise does not introduce very strong effects, so that the "optimum filter" is not appropriate. As we have described above, we would like to get rid of high frequency Fourier components of the spectrum not because of the noise, but because of the bad aliasing problems brought about by the unresolved steep gradient regions of the deconvolved image. We have decided to eliminate the Fourier components with frequencies somewhat lower than the Nyquist frequency by using a "Welch window" filter function:

$$F_j = \begin{cases} 1 - [(j-1)/(n-1)]^2 & ; \ j \leqslant n \\ 0 ; & j > n , \end{cases}$$
(2)

where F_j are the values of the filter function to be used in equation (1), j is the wavenumber, and n is the value of the wavenumber above which all Fourier components are completely eliminated by the filter. We have defined in equation (2) a "Welch window" filter in one dimension, but an extension to two dimensions can be calculated as $F_{i,j} = F_i \times F_j$, where F_i and F_j are both given by equation (2). The problem with this procedure is that one has to decide in a somewhat arbitrary way on a value for the cutoff wavenumber n (see eq. 2). Before deciding what value should be used for the cutoff wavenumber, let us discuss the effect obtained with different values of n.

Let us consider a one dimensional boxcar test function:

$$h_k = \begin{cases} 1 ; & -2 \leqslant k \leqslant 2 \\ 0 ; & \text{otherwise.} \end{cases}$$
(3)

This function shows in a very radical way the problems found in our CCD images. It shows a not very well resolved peak (only five pixels across) and completely
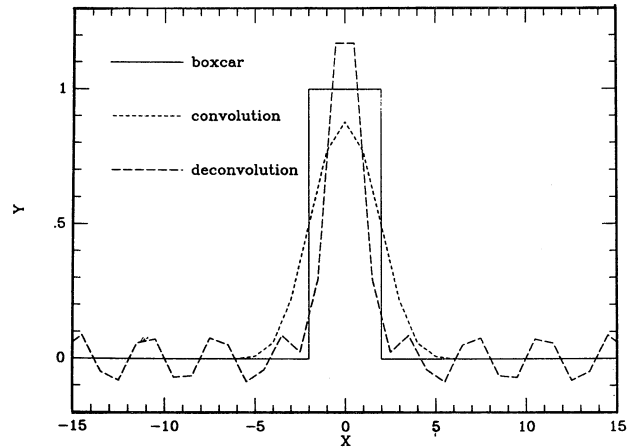

Fig. 1. From a function calculated by convolving a boxcar with a Gaussian function (of FWHM = 3) we have deconvolved the Gaussian profile. A total number of 64 grid points was used (the separation between grid points was $\Delta X = 1$), so that 33 Fourier components were obtained. In the plot we see the original boxcar function, the convolution of the boxcar with the simulated Gaussian "seeing profile", and the results from a deconvolution obtained with no filtering.

unresolved high gradient regions (i.e. the vertical sides of the boxcar). A grid of 64 pixels has been used. We have convolved this boxcar function with a simulated seeing profile:.a Gaussian with a FWHM of 3 pixels (in the case of our CCD frames, the seeing profile is always obtained from a bright but unsaturated stellar image, and a seeing of approximately one second of arc roughly corresponds to two or three pixels). In this way we generate a "simulated observation" g, from which we attempt to deconvolve the seeing profile.

In Figure 1, we see the original boxcar function (see eq. 3), the convolution (carried out by direct integration) of the boxcar function with a 3 pixel FWHM Gaussian, and the resulting unfiltered deconvolution. We see that if the deconvolution is carried out with all of the 33 Fourier components which are obtained (without any filtering whatsoever), a function that shows a peak at the position of the boxcar and strong oscillations in the rest of the computational grid is obtained (see Figure 1). This solution is obviously unacceptable. If we apply the filter given by equation (3) with a cutoff wavenumber $n = 25$, a solution that shows a much broader peak at the position of the boxcar, and strongly reduced oscillations is obtained (see Figure 2). If we use a filter function with a cutoff wavenumber $n = 18$, the oscillations are more strongly damped, but decreasing the cutoff wavenumber even further (to $n = 13$, see Figure 2) has the effect of slightly increasing the amplitude of these oscillations.

In other words, if one carries out deconvolutions with increasing degrees of filtering (i.e. with decreasing values of n) a decrease in the amplitude of the oscilla-
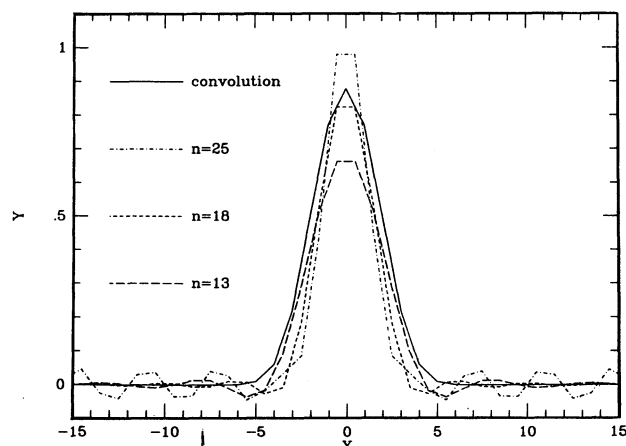
Fig. 2. Deconvolution of the seeing profile for the test function shown in Figure 1 (also see the text). Deconvolutions with filters of cutoff wavenumbers $n = 25, 18$ and 13 are shown.

Even though for the example which we have discussed above an improvement in the spatial resolution is indeed obtained, this improvement is not very impressive. The deconvolution process does not produce the steep sides and flat top of the original boxcar function. For tests with boxcar functions convolved with Gaussians of increasing width, an even smaller improvement of the spatial resolution (or even no improvement at all) is obtained.

On the other hand, the observed CCD images present somewhat less severe problems that the boxcar functions described above. In general, our CCD images of H-H objects present few bright condensations (sometimes almost merged with each other) surrounded by a more extended, diffuse background. We have tried to simulate such a situation with the test function:

$$h_k = exp(k - 5/2)^2/9 + exp(k + 5/2)^2/9 + (1/10)exp(k/20)^2 . \qquad (4)$$

tions is first observed, until a minimum amplitude is obtained. If the value of n is decreased even further, the amplitude of the oscillations starts to slowly increase again. By carrying out deconvolutions with different values of n, we can choose the result with the lowest value for the amplitude of the oscillations. In the case of our boxcar test function (see equation (3), and Figures 1 and 2), the oscillations of minimum amplitude are obtained for cutoff wavenumbers in the range $n = 15 - 18$. In Figure 3, the full width half maximum (FWHM) of the deconvolved function is shown as a function of the cutoff wavenumber n used for the deconvolution. For the range $n = 15 - 18$, the FWHM of the deconvolved function approximately coincides with the width of the original boxcar function.

This function shows two strong peaks (of FWHM ≈ 3 pixels) with a separation of approximately 5 pixels, and a weak, more extended "background" (see Figure 4. Again we have considered a domain of 64 pixels. We have convolved this function with a FWHM = 3 pixels Gaussian, and then carried out a deconvolution in the way described above. We find that the lowest amplitude ripples are obtained with a filter of cutoff wavenumber $n \approx 18$, and we show the results which were obtained with this filter in Figure 4.

The results obtained for this test function (equation 4) are as follows. In the deconvolved function, the width of the two peaks is very similar to the width of the corresponding peaks in the original function (see equation 4 and Figure 4). On the other hand, in
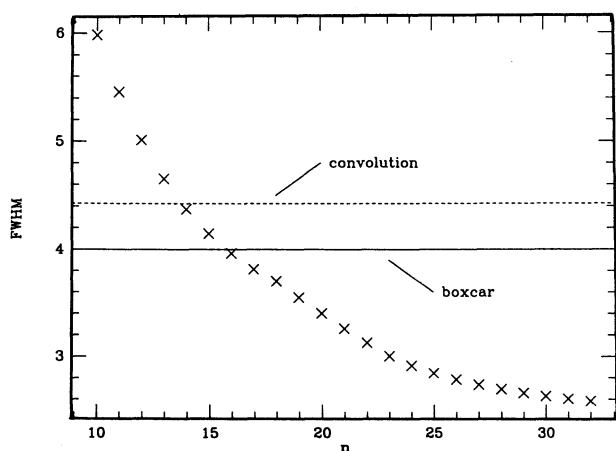

Fig. 3. FWHM of the deconvolved test function as a function of the cutoff wavenumber n used in the deconvolution (see the text). Also shown are the width of the original boxcar function, and the FWHM of the result of convolving the boxcar with the simulated seeing profile.
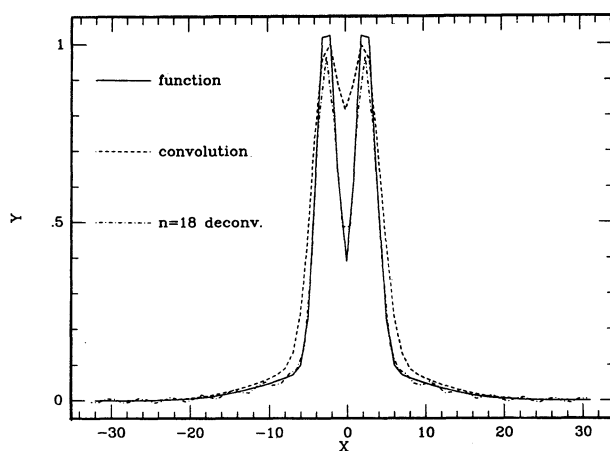

Fig. 4. Results obtained for a second test function, which consists of a superposition of three Gaussians (see the text). The original function, the result of the convolution with the simulated seeing profile, and the result obtained from the deconvolution process are shown.

the deconvolved function the two peaks are not as high and the valley between the two peaks not as deep as in the original function. Nevertheless, a considerable improvement in the spatial resolution (with respect to the "convolved" function) is obtained. The general shape of the "background" (determined by the third term of equation 4) is restored quite well by the deconvolution process (because no filtering of low frequency Fourier components is made), but a periodic ripple structure is superimposed on the deconvolved background (see Figure 4). These ripples are a result of aliasing of high frequency components of the Fourier spectrum, which correspond to the steep sides of the two peaks of the test function.

In practice, this contamination of the diffuse background by ripples resulting from narrow, high intensity peaks puts a limit on the low intensity cutoff which one can use for displaying deconvolved CCD images. Contours of low enough intensity always show periodic ripple structures which radiate away from the high intensity peaks, confusing the information about the diffuse background found in the deconvolved image. To avoid showing somewhat confusing images, we have chosen to present our results as constant intensity contour plots in which the lowest intensity contour lies above the peaks of these ripple structures. In this way, we loose a large part of the information about the diffuse background found in the original deconvolved images.

This is the process we have used for the deconvolution of the seeing profile from our two-dimensional CCD images. We have carried out deconvolutions with decreasing values for the cutoff wavenumber n, and then chosen the deconvolved image with lowest amplitude residual oscillations. In the case of actual observations it is of course not so easy to decide what features are oscillations due to aliasing problems, and what features correspond to real structures of the observed object. Just the same, it is possible (at least to some degree) to recognize most real features because of their lack of periodicity.

The difficulty in separating real features from spurious oscillations results in some uncertainty in the determination of the optimum value for the cutoff wavenumber n. Because of this, we have decided to always show the results for two different values of n: a "high resolution" (higher n) image and a "low resolution" (lower n) image. Both values of the cutoff wavenumber n have been chosen so that the amplitude of the residual oscillations is low.

The elimination of oscillations (due to aliasing problems) can be carried out (as described above) only at the expense of decreasing the spatial resolution of the deconvolved image (see Figure 1). This problem (which is brought about by the relatively low oversampling of our CCD images) implies that the effect of the seeing can be deconvolved from the observed images only in an approximate way. Just the same, a modest increase in the spatial resolution of the images can be obtained.

III. DISCUSSION OF THE RESULTS

a) The HH 2 Hα Image

We have obtained an Hα image of the H-H objects HH 1 and 2 under excellent seeing conditions (a FWHM of 0.88″, see Table 1). Let us first discuss the results obtained for the object HH 2.

Because HH 2 is one of the brightest H-H objects, it has been quite extensively observed in the past. This object shows a very remarkable, high contrast condensation structure (see e.g., Herbig 1974). It has been found that these condensations have different proper motions (Herbig and Jones 1981), and also show a quite drastic time-variability (Herbig 1969).

Theoretical interpretations of the condensation structure of HH 2 are generally based on the assumption that each condensation corresponds to a bow shock formed around a separate "interstellar bullet" (Hartmann and Raymond 1984; Choe 1984; Cantó and Rodríguez 1986; Hartigan, Raymond and Hartmann 1987). A different scenario has been proposed by Lightfoot and Glencross (1986a), who have modelled HH 2 as a "wobbling jet" that collides with gaseous "obstacles" and is deflected a number of times (the positions of the condensations correspond to the places where the jet is deflected). Raga and Böhm (1987) have suggested that the condensation structure of HH 2 might be the result of thermal instabilities in the recombination region of a *single* bow shock, but it is still not clear whether or not such a model can explain the observational results obtained for HH 2 (see e.g., Cantó and Rodríguez 1986).

Several radio, infrared and optical studies of the region around HH 1 and 2 have been carried out. One of the most interesting aspects of such work has been the discovery of what appears to be the source of the HH 1/2 system (Pravdo et al. 1985) and the study of the region surrounding the source (Strom et al. 1985; Bohigas et al. 1985; Tapia et al. 1987).

In Figure 5a, we see the Hα map obtained from our CCD frame. The abscissa is oriented parallel to the axis of the HH 1/2 system and points away from the source (a direction corresponding to a position angle of 148°). Because of the good seeing conditions, the condensations are well separated. We have labeled the condensations as A, B, C, D, E, G, H, I, K and M, following the notation of Herbig and Jones (1981). The condensation labeled L by Herbig and Jones (1981) lies outside our CCD frame. We have also detected a condensation which we have labeled with the letter P (see Figure 5a), which is visible in the more recent of the photographic images of Herbig and Jones (1981), but has not been labeled by these authors.

In Figure 5b, we see a "reconstructed" Hα intensity map, obtained by deconvolving the seeing profile form the observed image (with the method described in § II)

and convolving back again the resulting frame with the seeing profile. It is clear that the structures observed in the intensity maps 5a and 5b are almost identical, except for the fact that the peaks of the condensations in 5b are somewhat lower. This effect is brought about by the loss of power in the peaks due to the filtering which

has been carried out in the deconvolution (see § II and Figure 1). We show Figure 5b because in some measure it represents qualitatively the errors involved in the deconvolution process.

Figures 5c and 5d show the intensity maps obtained after a deconvolution of the seeing from the original ob-
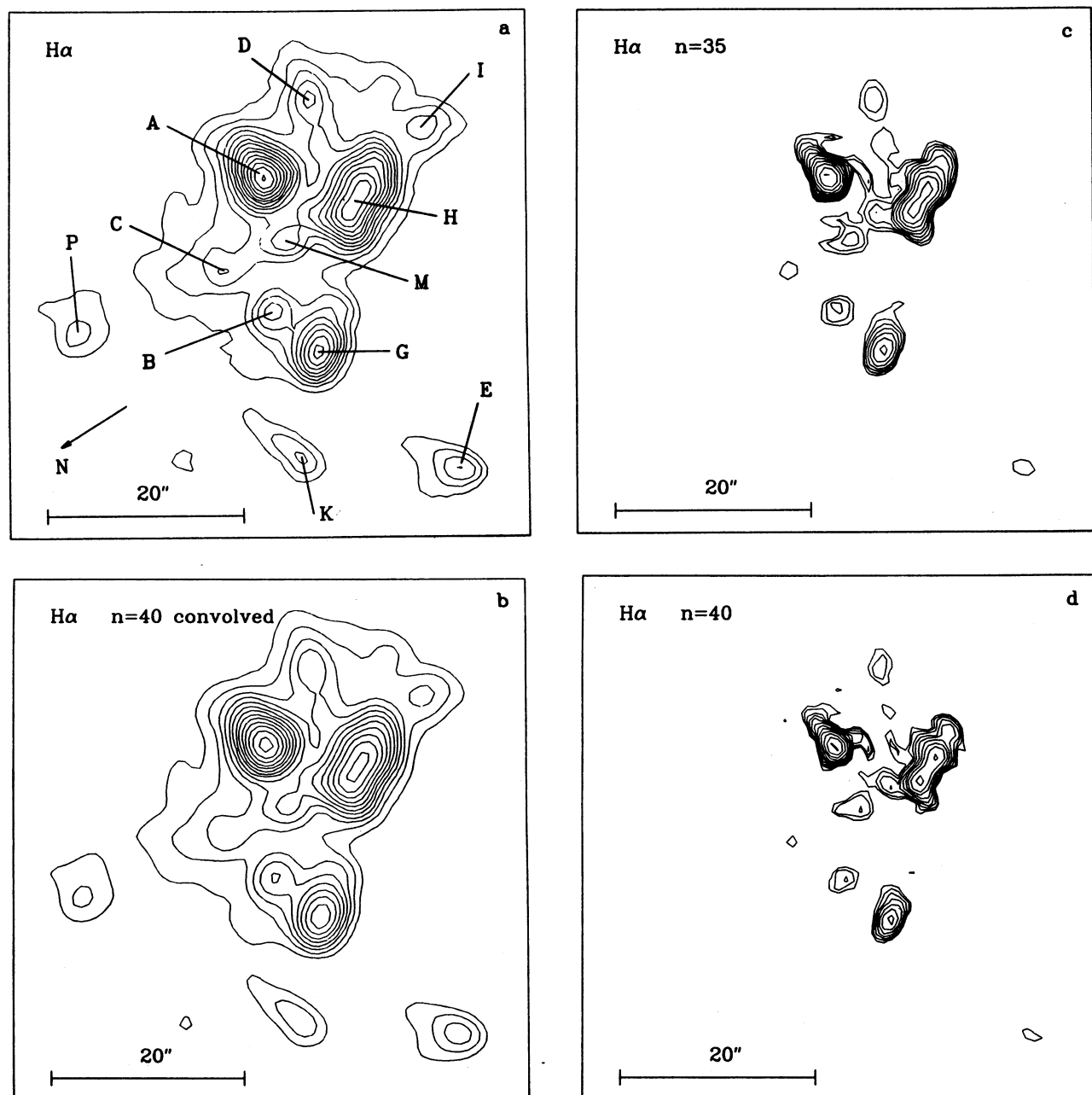
Fig. 5. Hα intensity maps of HH 2. The abscissa is approximately parallel to the axis of the HH 1/2 system (a position angle of 148°). The deconvolution of the seeing profile has been carried out on a 128 × 128 pixel subset of the original CCD frame. We show: (a) the original intensity map; (b) the reconstructed image, obtained by deconvolving the seeing profile and convolving it back again; (c) the low resolution deconvolution (using a $n = 35$ filter, which eliminates all Fourier components with wavelengths $\leqslant \Delta X_{min} = 1.4''$); and (d) the high resolution deconvolution (using a $n = 40$ filter, which eliminates all Fourier components with wavelengths $\leqslant \Delta X_{min} = 1.2''$, see text). Two successive contours represents an intensity ratio of $2^{1/2}$.

servation. Figure 5c is a "low resolution" map, obtained using a filter with $n = 35$ (the total number of Fourier components was 65), which cuts off the Fourier components with spatial wavelengths $\Delta X \leqslant \Delta X_{min} = 1.4''$. Figure 5d is a "high resolution" map, obtained using a filter with $n = 40$, which cuts off the Fourier components with spatial wavelengths $\Delta X \leqslant \Delta X_{min} = 1.2''$. Both values for the cut off wavenumber n were chosen so that the residual oscillations in the deconvolved image were small (see § II).

Figures 5c and 5d show several interesting effects. The condensations naturally are spatially less extended than in the observed image (see Figure 5a). Condensation H appears well separated into two components, confirming the results of Herbig and Jones (1981). The NW component of condensation H was very faint in 1959, and had become considerably brighter by 1980 (see Herbig and Jones 1981). The two components of H now appear to have approximately the same intensity, with the NW component being marginally brighter.

If the "multiple-bow shock" picture of HH 2 is correct, one would have expected to see separate condensations showing structures similar to the intensity maps of bow shocks predicted by Raga (1986). The fact that no "bow shock-like" structures are observed does not imply that a multiple-bow shock model is not applicable for HH 2. The bow shocks around separate interstellar bullets could still be unresolved in our enhanced spatial resolution images. A somewhat more severe problem for this interpretation of HH 2 appears to be the fact that in the deconvolved images (Figures 5c and 5d) the condensations are not completely separated, but appear to be joined by "bridges" of emitting material (the most notable being the connection between condensations H and A).

At this time, it is not clear what these structures (connecting separate condensations) actually are. In principle, they could be the result of line of sight projection effects of structures formed by several independent condensations (which could still be attributed to separate "interstellar bullets"). These connecting structures could also be the result of considerably different flows, such as the ones suggested by Lightfoot and Glencross (1986a) or by Raga and Böhm (1987). In order to decide which model provides a better explanation for the complex intensity maps obtained for HH 2, detailed studies of predictions from different models will have to be carried out.

b) *The HH 1 Hα Image*

The Hα CCD frame described in the previous section also contains an image of the H-H object HH 1. This object is situated at approximately the same distance from the source as HH 2, but in the opposite direction (see e.g., Bohigas *et al.* 1985). A line pointing from the source toward HH 1 has a position angle of approximately $-32°$.

As is the case for HH 2, several models have been proposed for HH 1. For example, Hartigan, Hartmann, and Raymond (1987) have proposed a "multi-bow shock" model, Lightfoot and Glencross (1986a) have proposed a "wobbling jet" model, and Böhm and Solf (1985) have proposed a "single-bow shock" model. These are the same models that have been proposed for HH 2 (see § III.a), but in the case of HH 1 they have to explain somewhat different observational properties.

In Figure 6a we see the Hα image of HH 1. The abscissa is again approximately parallel to a line joining the source with the H-H object (with a position angle of $-32°$). Following the notation of Herbig and Jones (1981), we have labeled the observed condensations with the letters F, D, C, and A (we do not observe any trace of Herbig and Jones' condensation B). We observe a faint condensation (not labeled by Herbig and Jones 1981), which we have labeled with a letter G.

In Figure 6b, we show the intensity map obtained by deconvolving the seeing from the observed image, and then convolving it back again. We again see the loss in the peak intensity of the condensations which is a result of the filtering carried out in the deconvolution.

In Figures 6c and 6d, we show "low resolution" and "high resolution" (see § III.a) deconvolved images. As a result of the deconvolution of the seeing profile, a new condensation appears in the region between condensations D and G (see Figures 6a and 6d). The contrast between the condensation and their environment is also increased, but it is clear that the condensations are still interconnected by radiating material.

Raga *et al.* (1987) have shown that a model of a single, time-dependent radiating bow shock (formed by the head of a jet or by an interstellar bullet) can explain a large number of the observational properties of HH 1. The theoretical predictions agree in a qualitative way with position-velocity diagrams (Böhm and Solf 1985), narrow-band CCD images (Raga *et al.* 1987), and proper motions (Herbig and Jones 1981) observed for HH 1. This successful prediction of the properties of HH 1 appears to be at this time one of the most complete interpretations of observations of any H-H object.

Our enhanced resolution intensity maps of HH 1 (Figures 6c and 6d) show a good qualitative agreement with the predictions from the bow shock model of Raga *et al.* (1987). This comparison between predicted and observed intensity maps shows a considerably better agreement between theory and observations than had been obtained by Raga *et al.* (1987) (who have not applied image reconstruction techniques in the reduction of the data).

c) *The HH 47A [S II] 6717+ 6731 Image*

We have reanalized the [S II] 6717+6731 CCD image of HH 46/47 of Raga and Mateo (1987), carrying out a deconvolution of the seeing profile. Unfortunately, except for the region with HH 47A, the signal-to-noise ratio of this frame is too low for the purpose of carry-
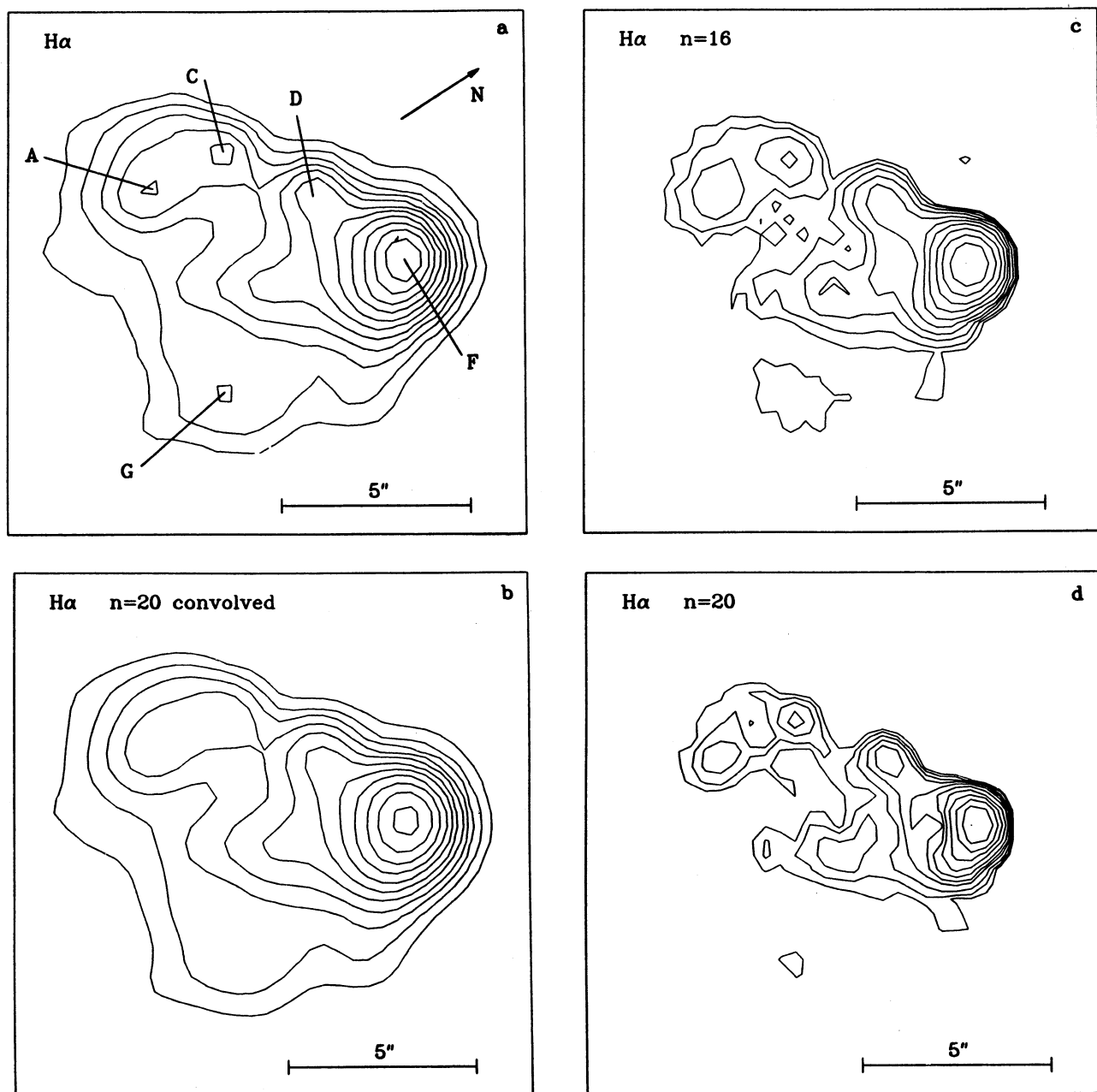
Fig. 6. Hα intensity maps of HH 1. The abscissa is approximately parallel to the axis of the HH 1/2 system (a position angle of $-32°$). The deconvolution of the seeing profile has been carried out on a 64 × 64 pixel subset of the original CCD frame. We show: (a) the original intensity map; (b) the reconstructed image (obtained by deconvolving the seeing profile and convolving it back again); (c) the low resolution deconvolution (using a $n = 16$ filter, which eliminates all Fourier components with wavelengths $< \Delta X_{min} = 1.5''$); and (d) the high resolution deconvolution (using a $n = 20$ filter, which eliminates all Fourier components with wavelengths $< \Delta X_{min} = 1.2''$, see text). Two successive contours represent an intensity ratio of $2^{1/2}$.

ing out such a deconvolution. Because of this, we have limited our analysis to the bright object HH 47A.

In Figure 7a, we see the observed intensity map; in Figure 7b, the reconstructed image (deconvolution + convolution of the seeing profile; in Figure 7c a "high resolu-tion" deconvolved image, and in Figure 7d a "low resolution" deconvolved intensity map. Again the abscissa is oriented parallel to the axis of the system of H-H objects (with a position angle of approximately 55.5°).
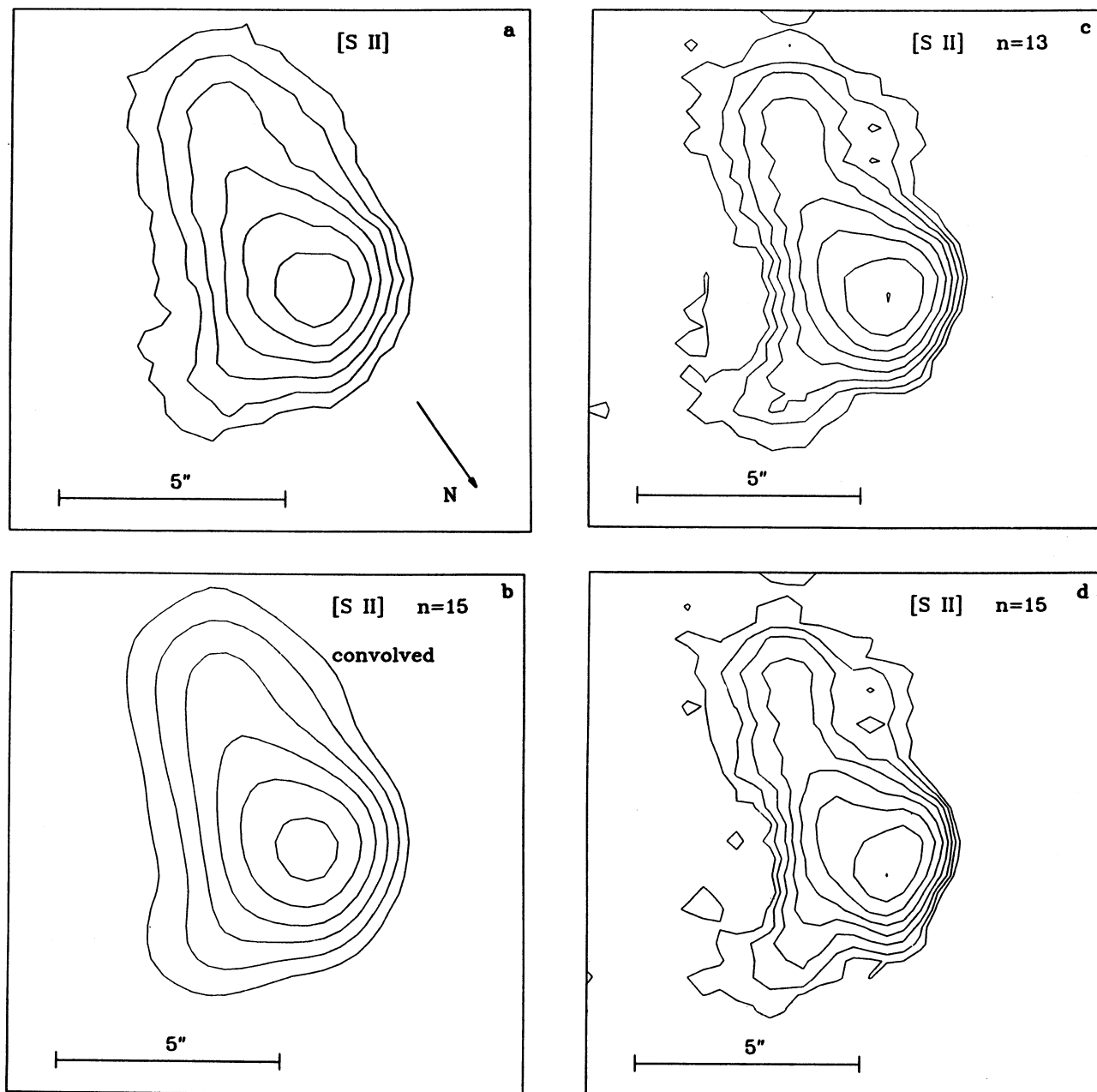
Fig. 7. [S II] 6717 + 6731 intensity maps of HH 47A. The abscissa is approximately parallel to the axis of the HH 46/47 system (a position angle of 55.5°). The deconvolution of the seeing profile has been carried out on a 64 × 64 pixel subset of the original CCD frame. We show: (a) the original intensity map; (b) the reconstructed image (obtained by deconvolving the seeing profile and convolving it back again; (c) the low resolution deconvolution (using a $n = 13$ filter, which eliminates all Fourier components with wavelengths $\leqslant \Delta X_{min} = 1.8''$); and (d) the high resolution deconvolution (using a $n = 15$ filter, which eliminates all Fourier components with wavelengths $\leqslant \Delta X_{min} = 1.5''$, see text). Two successive contours represent an intensity ratio of $2^{1/2}$.

The high spatial resolution intensity map of HH 47A (Figure 7d) shows a structure which is not very different from the direct observational image (Figure 7a). It appears that naively one might divide HH 47A into two components: the condensation that corresponds to the intensity maximum of HH 47A, and an elongated structure approximately perpendicular to the axis of symmetry of the HH 46/47 system (i.e. the abscissa of Figure 7).

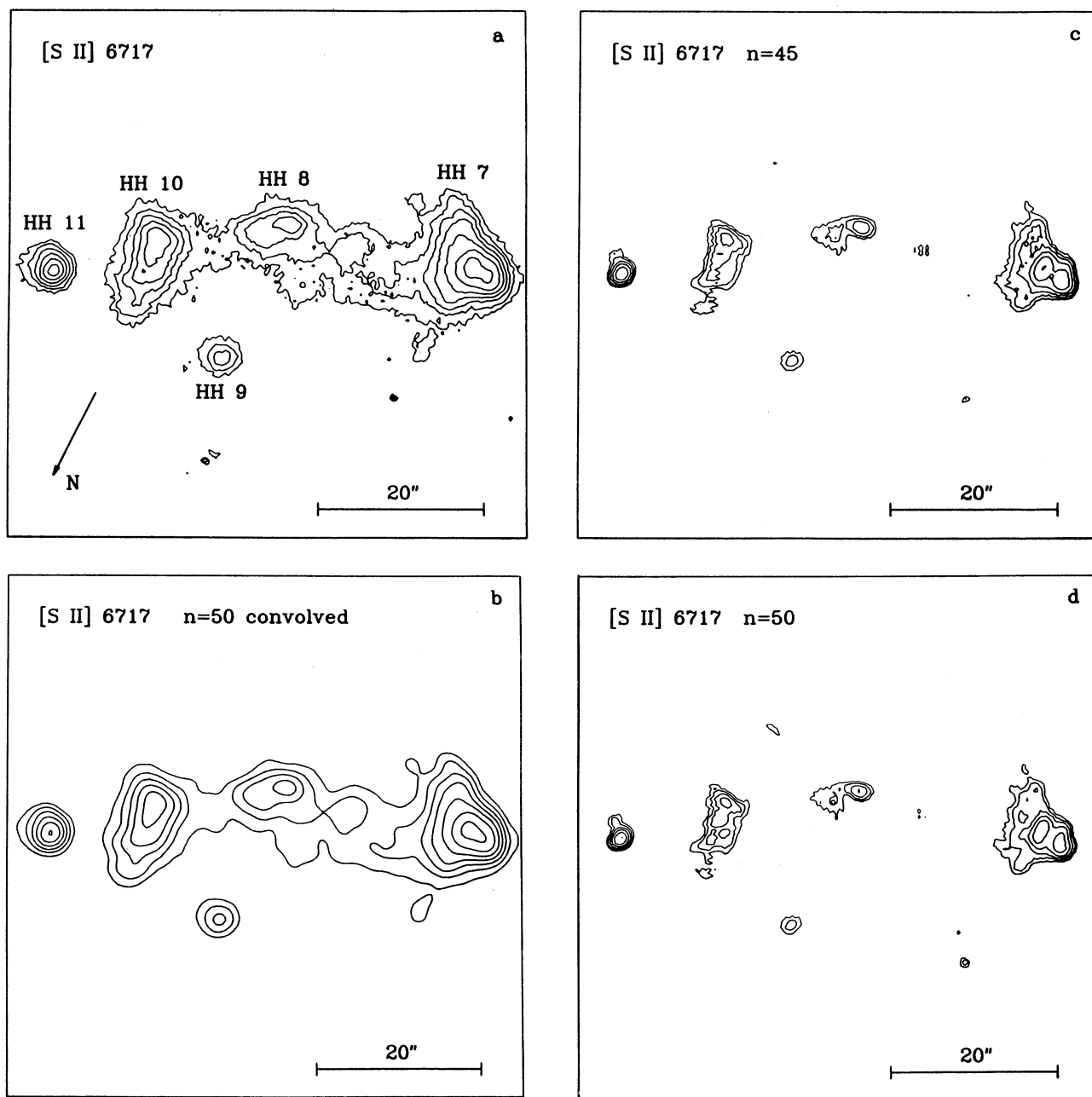It is not clear which model might explain this spatial

Fig. 8. [S II] 6717 intensity maps of HH 7-11. The abscissa is approximately parallel to the axis of the HH 7-11 system (a position angle of 117°). The deconvolution of the seeing profile has been carried out on a 256 × 256 pixel subset of the original CCD frame. We show: (a) the original intensity map; (b) the reconstructed image (obtained by deconvolving the seeing profile and convolving it back again); (c) the low resolution deconvolution (using a $n = 45$ filter, which eliminates all Fourier components with wavelengths $\leqslant \Delta X_{min} = 2.2''$); and (d) the high resolution deconvolution (using a $n = 50$ filter, which eliminates all Fourier components with wavelengths $\leqslant \Delta X_{min} = 1.9''$, see text). Two successive contours represent an intensity ratio of $2^{1/2}$.

structure. For example, Meaburn and Dyson (1987) have suggested that HH 47A corresponds to the head of the HH 46/47 jet. This scenario appears to fit nicely with the general morphology of HH 46/47, but it is presently not clear whether or not this model can explain the very low excitation spectrum observed in HH 47A (see e.g., Dopi-

ta 1978; Graham 1986; Raga and Mateo 1987). We note that the spatial structure observed in the high resolution images of HH 47A (Figures 7c and 7d) does not agree well with the predictions from bow shocks models (Raga 1986; Raga et al. 1987). From this, one can conclude that if HH 47A does correspond to the head of a jet, the

bow shock formed by the head of the jet produces at most only part of the observed intensity distribution.

d) *The HH 7-11 [S II] 6717 Image*

We have obtained a [S II] 6717 CCD frame of the HH 7-11 system under moderate seeing conditions (a FWHM of $1.63''$ see Table 1). In Figure 8, we show the observed intensity map (Figure 8a), the reconstructed image deconvolution + convolution of the seeing profile, Figure 8b), a "high resolution" deconvolved image (Figure 8c) and a "low resolution" deconvolved intensity map (Figure 8d). Again the abscissa is oriented parallel to the axis of the system of H-H objects (with a position angle of approximately $117°$). We have defined the axis of the HH 7-11 system as a line joining the intensity maximum of HH 7 with maximum of HH 11 (see Figure 8a). The infrared source SSV 13 (which is generally assumed to be the source of the HH 7-11 system, see e.g., Strom, Vrba, and Strom 1974) is located approximately $5''$ to the north of this axis.

In the high spatial resolution intensity maps we observed several interesting effects. HH 11 (see Figure 8a) still appears to be unresolved in the deconvolved images (Figures 8c and 8d). This is nothing short of surprising given the fact that Solf and Böhm (1987) have observed the existence of velocity gradients across this object. Also quite remarkable is the clear separation of HH 7 into two condensations (Figure 8d).

The HH 7-11 system of H-H objects appears to be more complex and less well understood that the HH 1/2 and HH 46/47 systems. Very intriguing results have been obtained by Rudolph and Welch (1987), who have detected HCO^+ emission with very low radial velocity from this system of H-H objects. In Figure 9, we show the observations of Rudolph and Welch (1987), superimposed on our high resolution image of HH 7-11. We confirm the results of Rudolph and Welch (1987) who found that the HCO^+ emission shows condensations which do not coincide spatially with the optical condensations (their results were based on a comparison with a lower spatial resolution optical image). These authors have suggested that the observed configuration might be explained with a scenario in which a high velocity stellar wind is shocked against high density clumps (which are visible in HCO^+). The optical emission would come from the shocks in the stellar wind, which would form in the upstream side (i.e. toward the source of the HH 7-11 system) of the clumps. The morphology of HH 10 (and of its HCO^+ counterpart) appears to agree with what one would expect from such a scenario, but such an agreement is not so clear in the case of the other H-H objects. In particular, HH 7 appears not to have any HCO^+ counterpart whatsoever.

Other authors have proposed different explanations for the complex optical structure of the HH 7-11 system (see e.g., Lightfoot and Glencross 1986b; Solf and Böhm 1987) than the one described above. We believe
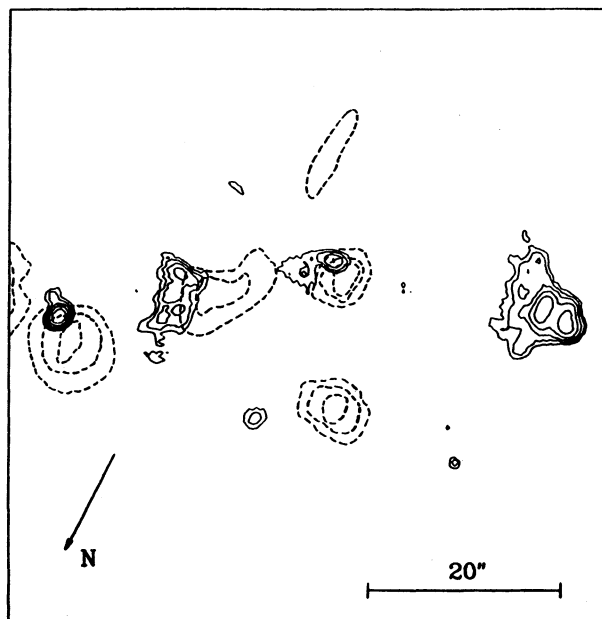

Fig. 9. The "high resolution" [S II] 6717 intensity map of HH 7-11 (solid contours, see also Figure 5) is shown superimposed on the HCO^+ (J = 1 $\Rightarrow$ 0) image (dashed contours) of Rudolph and Welch (1987).

that while our high spatial resolution intensity maps do provide new information about the structure of HH 7-11, this information does not show in a conclusive way which of the proposed scenarios for these H-H objects is actually correct.

IV. CONCLUSIONS

We have shown that image reconstruction techniques are useful even in the case of not highly oversampled CCD images. A moderate improvement of the spatial resolution can be obtained with a rather small computational effort. This is particularly interesting for the case of Herbig-Haro objects, which many times show a structure of marginally resolved condensations.

Of the H-H objects which have been studied, the most interesting results have been obtained for HH 1. We find that the high spatial resolution intensity maps of this object agree qualitatively very well with predictions from the time-dependent bow shock models of Raga *et al.* (1987). The agreement of model predictions with these observational results strengthens the case for a single-bow shock model of HH 1.

For HH 2, we have found that the condensations are not resolved in the high spatial resolution intensity maps. We find interconnecting structures which appear to be joining some of the separate condensations. In order to explain this structure, rather complex hydrodynamical models might be needed.

In the case of HH 47A we have found that the high resolution images do not appear to resemble the predic-

tions from bow shock models (see e.g., Raga 1986). This result implies that if HH 47A does correspond to the head of the HH 46/47 jet, at least a considerable fraction of the emission is produced in shocks other than the bow shock.

The high resolution maps of HH 7-11 confirm the lack of coincidence between the optical H-H objects and their HCO$^+$ counterparts found by Rudolph and Welch (1987). The scenario proposed by these authors (a stellar wind which is shocked against high density clumps of gas) appears to at least partially explain the morphology of this system of H-H objects.

REFERENCES

Bohigas, J. et al. 1985, Rev. Mexicana Astron. Astrof., 11, 149.
Böhm, K. H. and Solf, J. 1985, Ap. J., 294, 533.
Brault, J. W. and White, O. R. 1971, Astr. and Ap., 13, 169.
Cantó, J. 1980, Astr. and Ap., 86, 327.
Cantó, J. and Rodríguez, L.F. 1986, Rev. Mexicana Astron. Astrof., 13, 57.
Cantó, J., Sarmiento, A., and Rodríguez, L.F. 1986, Rev. Mexicana Astron. Astrof., 13, 107.
Choe, S.-U 1984, Ph. D. thesis, University of Minnesota.
Choe, S.-U., Böhm K. H., and Solf, J. 1985, Ap. J., 288, 338.
Dopita, M. A. 1978, Ap. J. Suppl., 37, 117.
Dyson, J. 1984, Ap. and Space Sci., 106, 181.
Falle, S.A.E.G., Innes, D.E., and Wilson, M.J. 1987, M.N.R.A.S., 225, 741.
Graham, J.A. 1986, Ap. J., 302, 352.
Haro, G. 1952, Ap. J., 115, 572.
Haro, G. 1953, Ap. J., 117, 73.
Hartigan, P., Raymond, J.C., and Hartmann, L. 1987, Ap. J., 316, 323.
Hartmann, L. and Raymond, J.C. 1984, Ap. J., 288, 338.
Hawkins, M.R.S. 1979, Astr. and Ap., 76, 46.
Herbig, G.H. 1951, Ap. J., 113, 697.
Herbig, G.H. 1952, J. Roy. Astr. Soc. Canada, 46, 222.
Herbig, G.H. 1969, in Non-Periodic Phenomena in Variable Stars, (ed.) L. Detre (Academic Budapest), p. 75.
Herbig, G.H. 1974, Lick Observatory Bull., 658.
Herbig, G.H. and Jones, B.F. 1981, A.J., 86, 1232.
Lightfoot, J.F. and Glencross, W.M. 1986a, M.N.R.A.S., 221, 47p.
Lightfoot, J.F. and Glencross, W.M. 1986b, M.N.R.A.S., 221, 993.
Meaburn, J. and Dyson, J.E. 1987, M.N.R.A.S., 225, 863.
Mundt, R. 1985, in Protostars and Planets, Vol. 2, (ed.) B.C. Black and M.S. Matthews (Tucson: University of Arizona Press), p. 414.
Narayan, R. and Nityananda, R. 1986, Ann. Rev. Astr. and Ap., 24, 117.
Norman, C.A. and Silk, J. 1979, Ap. J., 228, 197.
Pravdo, S.H. et al. 1985, Ap. J. (Letters), 293, L35.
Raga, A.C. 1986, A.J., 92, 637.
Raga, A.C. and Böhm, K.H. 1987, Ap. J., in press.
Raga, A.C. and Mateo, M. 1987, A.J., 94, 684.
Raga, A.C. and Mateo, M. 1988, A.J., in press.
Raga, A.C., Mateo, M., Böhm, K.H., and Solf, J. 1987, A.J., submitted.
Reipurth, B., Bally, J., Graham, J.A., Lane, A., and Zealy, W.J. 1986, Astr. and Ap., 164, 51.
Rudolph, A. and Welch, W.J. 1987, Ap. J. (Letters), in press.
Schwartz, R.D. 1978, Ap. J., 223, 884.
Solf, J. and Böhm, K.H. 1987, A.J., 93, 1172.
Solf, J., Böhm, K.H., and Raga, A.C. 1986, Ap. J., 305, 795.
Strom, S.E. et al. 1985, A.J., 90, 2281.
Strom, K.M., Strom, S.E., Wolff, S., Morgan, J., and Wenz, M. 1986, Ap. J. Suppl., 62, 39.
Strom, S.E., Vrba, F.J., and Strom, K.M. 1974, A.J., 191, 111.
Tapia, M., Roth, M., Carrasco, L., and Ruiz, M.T. 1987, M.N.R.A.S., 224, 587.

M. Mateo and Alejandro C. Raga: Astronomy Department FM-20, University of Washington, Seattle, WA. 98195 USA.